Inhibition of Pyruvate Kinase M2 by Reactive Oxygen Species Contributes to Cellular Antioxidant Responses

Dimitrios Anastasiou *et al.*

Science **334**, 1278 (2011);
DOI: 10.1126/science.1211485

Science (print ISSN 0036-8075; online ISSN 1095-9203) is published weekly, except the last week in December, by the American Association for the Advancement of Science, 1200 New York Avenue NW, Washington, DC 20005.

an IPM (*29*), but we are unaware of any field studies where drivers have been identified for all functions. Even if environmental drivers are identified, predicting how they may change in the future is currently unfeasible, because the environment that populations experience is complex, consisting of abiotic and biotic drivers that can interact, sometimes nonlinearly (*30*). Currently, the best that can probably be done is to explore the consequences of environmental change scenarios. For example, if we assume changes that reduce the mean of each intercept by 10%, we predict decreases in mean population size and the strength of both viability and fertility selection; no change in coat color frequencies; and increases in the variance in population size, mean body size, and generation length. In reality, we have little idea of the extent to which environmental change will affect each function, because key environmental drivers have yet to be identified for all functions, and the dynamics of those that have been identified are not well understood (*24*–*26*).

Although accurate prediction is currently not possible, our results do reveal that, for Yellowstone wolves, (i) environmental change will inevitably generate eco-evolutionary responses; (ii) change in the mean environment will have more profound population consequences than changes in the environmental variance; and (iii) environmental change affecting different functions can generate contrasting eco-evolutionary dynamics. Because IPMs are sufficiently general and because density dependence and environmental variation affect most populations, these conclusions are likely to extend to other systems. The construction and analysis of IPMs across a range of systems may provide support for this proposition. In addition to providing a tool to explore eco-evolutionary dynamics, IPMs have also been extended to include spatial variation and to identify evolutionarily stable strategies (*21, 22*), giving them potential to unify several subdisciplines of population biology, including population ecology, quantitative genetics, population genetics, and life history theory. They have not yet been extended to incorporate processes that generate novel genetic variation; the results we report arise via the shuffling of existing phenotypic and genetic variation via selection and plasticity. Our findings suggest that existing phenotypic and genetic variation within Yellowstone wolves is sufficient for environmental change to generate substantial evolutionary change that will occur in tandem with shifts in wolf life history and population dynamics. Although accurate prediction of the eco-evolutionary consequences of environmental change is currently unfeasible for most natural populations, our results help explain why it so widespread, and perhaps inevitable.

References and Notes

1. T. M. Anderson *et al.*, *Science* **323**, 1339 (2009).
2. O. J. Schmitz, G. B. Kolenosky, *Can. J. Zool.* **63**, 1130 (1985).
3. B. E. Sæther, *Trends Ecol. Evol.* **12**, 143 (1997).
4. D. A. Miller, W. R. Clark, S. J. Arnold, A. M. Bronikowski, *Ecology* **92**, 1658 (2011).
5. T. W. Schoener, *Science* **331**, 426 (2011).
6. N. G. Hairston Jr., S. P. Ellner, M. A. Geber, T. Yoshida, J. A. Fox, *Ecol. Lett.* **8**, 1114 (2005).
7. D. Reznick, M. J. Butler IV, H. Rodd, *Am. Nat.* **157**, 126 (2001).
8. E. Post *et al.*, *Science* **325**, 1355 (2009).
9. J. A. Estes *et al.*, *Science* **333**, 301 (2011).
10. M. R. Easterling, S. P. Ellner, P. M. Dixon, *Ecology* **81**, 694 (2000).
11. J. A. Vucetich, D. W. Smith, D. R. Stahler, *Oikos* **111**, 259 (2005).
12. M. J. Kauffman, J. F. Brodie, E. S. Jules, *Ecology* **91**, 2742 (2010).
13. R. L. Beschta, W. J. Ripple, *Restor. Ecol.* **18**, 380 (2010).
14. J. A. Fuller, R. A. Garrott, P. J. White, *J. Wildl. Manage.* **71**, 1924 (2007).
15. T. P. Barnett *et al.*, *Science* **319**, 1080 (2008).
16. D. R. MacNulty *et al.*, *Ecol. Lett.* **12**, 1347 (2009).
17. D. R. MacNulty, D. W. Smith, L. D. Mech, L. E. Eberly, *J. Anim. Ecol.* **78**, 532 (2009).
18. T. Coulson, S. Tuljapurkar, D. Z. Childs, *J. Anim. Ecol.* **79**, 1226 (2010).
19. H. Caswell, *PLoS ONE* **6**, e20809 (2011).
20. M. Rees, S. P. Ellner, *Ecol. Monogr.* **79**, 575 (2009).
21. D. Z. Childs, M. Rees, K. E. Rose, P. J. Grubb, S. P. Ellner, *Proc. Biol. Sci.* **271**, 425 (2004).
22. P. B. Adler, S. P. Ellner, J. M. Levine, *Ecol. Lett.* **13**, 1019 (2010).
23. J. C. Pinheiro, D. M. Bates, *Mixed-Effects Models in S and S-PLUS* (Springer-Verlag, New York, 2000).
24. E. S. Almberg, L. D. Mech, D. W. Smith, J. W. Sheldon, R. L. Crabtree, *PLoS ONE* **4**, e7042 (2009).
25. L. D. Mech, D. W. Smith, K. M. Murphy, D. R. MacNulty, *J. Wildl. Manage.* **65**, 998 (2001).
26. D. W. Smith, T. D. Drummer, K. M. Murphy, D. S. Guernsey, S. B. Evans, *J. Wildl. Manage.* **68**, 153 (2004).
27. S. I. Candille *et al.*, *Science* **318**, 1418 (2007).
28. S. Tuljapurkar, C. C. Horvitz, J. B. Pascarella, *Am. Nat.* **162**, 489 (2003).
29. T. Coulson, P. Rohani, M. Pascual, *Trends Ecol. Evol.* **19**, 359 (2004).
30. T. Coulson, L. E. B. Kruuk, G. Tavecchia, J. M. Pemberton, T. H. Clutton-Brock, *Evolution* **57**, 2879 (2003).

Acknowledgments: T.C. acknowledges the European Research Council, the Wellcome Trust, the Royal Society, the Natural Environment Research Council, and the Wolfson Foundation for funding that supported the development of theory. D.R.M., R.K.W., and D.W.S. thank NSF for support (separate grants to R.K.W. and D.W.S.). Thanks to T. Ezard, J.-M. Gaillard, A. Malo, A. Ozgul, S. Schindler, I. Smallegange, and four anonymous reviewers for comments on an earlier version of the manuscript. D.W.S. and D.R.S. run the Yellowstone wolf project and along with D.R.M. conducted or oversaw all data collection. B.V. conducted genotyping under the supervision of R.K.W. D.R.M. and D.R.S. compiled the data file, and along with T.C. and D.W.S. planned model structure and statistical analyses. T.C. conducted analysis and modeling. T.C. and D.R.M. wrote the paper with input from all coauthors. Functional forms and parameter values for the model on which this paper is based are available in the SOM; data, results, and the R code to run simulations are available on Dryad (http://datadryad.org, doi:10.5061/dryad.bp23483h).

Supporting Online Material

www.sciencemag.org/cgi/content/full/334/6060/1275/DC1
Materials and Methods
SOM Text
Figs. S1 and S2
Tables S1 to S3
References (*31*–*45*)

7 June 2011; accepted 12 October 2011
10.1126/science.1209441

Inhibition of Pyruvate Kinase M2 by Reactive Oxygen Species Contributes to Cellular Antioxidant Responses

Dimitrios Anastasiou,[1,2] George Poulogiannis,[1,2] John M. Asara,[1,3] Matthew B. Boxer,[4] Jian-kang Jiang,[4] Min Shen,[4] Gary Bellinger,[1,5] Atsuo T. Sasaki,[1,2] Jason W. Locasale,[1,2] Douglas S. Auld,[4]* Craig J. Thomas,[4] Matthew G. Vander Heiden,[5,6] Lewis C. Cantley[1,2]†

Control of intracellular reactive oxygen species (ROS) concentrations is critical for cancer cell survival. We show that, in human lung cancer cells, acute increases in intracellular concentrations of ROS caused inhibition of the glycolytic enzyme pyruvate kinase M2 (PKM2) through oxidation of Cys^{358}. This inhibition of PKM2 is required to divert glucose flux into the pentose phosphate pathway and thereby generate sufficient reducing potential for detoxification of ROS. Lung cancer cells in which endogenous PKM2 was replaced with the Cys^{358} to Ser^{358} oxidation-resistant mutant exhibited increased sensitivity to oxidative stress and impaired tumor formation in a xenograft model. Besides promoting metabolic changes required for proliferation, the regulatory properties of PKM2 may confer an additional advantage to cancer cells by allowing them to withstand oxidative stress.

Control of the intracellular concentrations of reactive oxygen species (ROS) is critical for cell proliferation and survival. In cells treated with growth factors, transient increases in ROS concentrations are implicated in enhanced cell proliferation through inhibition of phosphotyrosine phosphatases and PTEN, which allows amplification of tyrosine kinase and phosphatidylinositol-3 kinase (PI-3K) signaling pathways (*1*). However, high concentrations of ROS can also damage cellular components and compromise cell viability (*2*). Tumor suppressor and oncogenic pathways frequently mutated in cancer commonly result in increased accumulation of ROS (*3*–*7*). Furthermore, conditions associated with tumorigenesis such as hypoxia, matrix detachment, mitochondrial dysfunction, and inflammation can all lead to excess production of ROS (*8*–*12*). Therefore, cancer cells are particularly challenged in dealing with oxidative stress (*2*, *13*).

Detoxification of ROS and the repair of oxidatively damaged proteins depend primarily on the availability of reduced glutathione (GSH). Glucose metabolism through the pentose phosphate pathway provides the reduced form of nicotinamide adenine dinucleotide phosphate (NADPH) to maintain glutathione in the reduced state (*14*, *15*). Glucose is also a major carbon source for biosynthetic processes (*16*). How glucose is metabolized in cancer cells is determined, in part, by expression of the glycolytic enzyme pyruvate kinase M2 (PKM2) (*17*). In contrast to its splice variant PKM1, which is expressed in many adult tissues, PKM2 is allosterically activated in a feed-forward regulatory loop by an upstream glycolytic metabolite, fructose-1,6-bisphosphate (FBP) and is susceptible to inhibition by growth factor signaling through interaction with phosphotyrosine-containing proteins (*18*). These properties of PKM2 allow proliferating cells to divert glucose into anabolic pathways emanating from glycolysis in order to meet the increased biosynthetic demands of proliferation.

Pyruvate kinase (PK) orthologs in many organisms, from bacteria to humans, are inhibited by oxidants (*19*–*22*). Exposure of A549 human lung cancer cells to 1 mM H_2O_2, 250 μM diamide (a thiol-oxidizing compound), or hypoxia (1% O_2) [which causes increased ROS production by mitochondrial complex III (*23*)] resulted in similar increases in intracellular concentrations of ROS (fig. S1) and caused decreases in PKM2 activity (Fig. 1, A and B) (*24*). In all cases, incubation of cell lysates with dithiothreitol (DTT), a strong reducing agent, restored PKM2 activity to nearly that of untreated cells, which indicated that the effects of treating cells with H_2O_2, diamide, or hypoxia on PKM2 activity reflect an oxidative event that is reversible with a thiol-reducing agent.

Association of PKM2 subunits into homotetramers is required for optimal enzymatic activity (*25*). Diamide treatment impaired coimmunoprecipitation of endogenous PKM2 with Flag-tagged PKM2, and this was reversed by adding DTT to the cell lysates before immunoprecipitation

[1]Beth Israel Deaconess Medical Center, Department of Medicine-Division of Signal Transduction, Boston, MA 02115, USA. [2]Department of Systems Biology, Harvard Medical School, Boston, MA 02115, USA. [3]Department of Medicine, Harvard Medical School, Boston, MA 02115, USA. [4]NIH Chemical Genomics Center, National Human Genome Research Institute, National Institutes of Health, 9800 Medical Center Drive, Rockville, MD 20850, USA. [5]Koch Institute for Integrative Cancer Research at Massachusetts Institute of Technology, Cambridge, MA 02139, USA. [6]Dana Farber Cancer Institute, Harvard Medical School, Boston, MA 02115, USA.

*Present address: Novartis Institutes for Biomedical Research, Center for Proteomic Chemistry, Cambridge, MA 02139, USA. †To whom correspondence should be addressed. E-mail: lewis_cantley@hms.harvard.edu

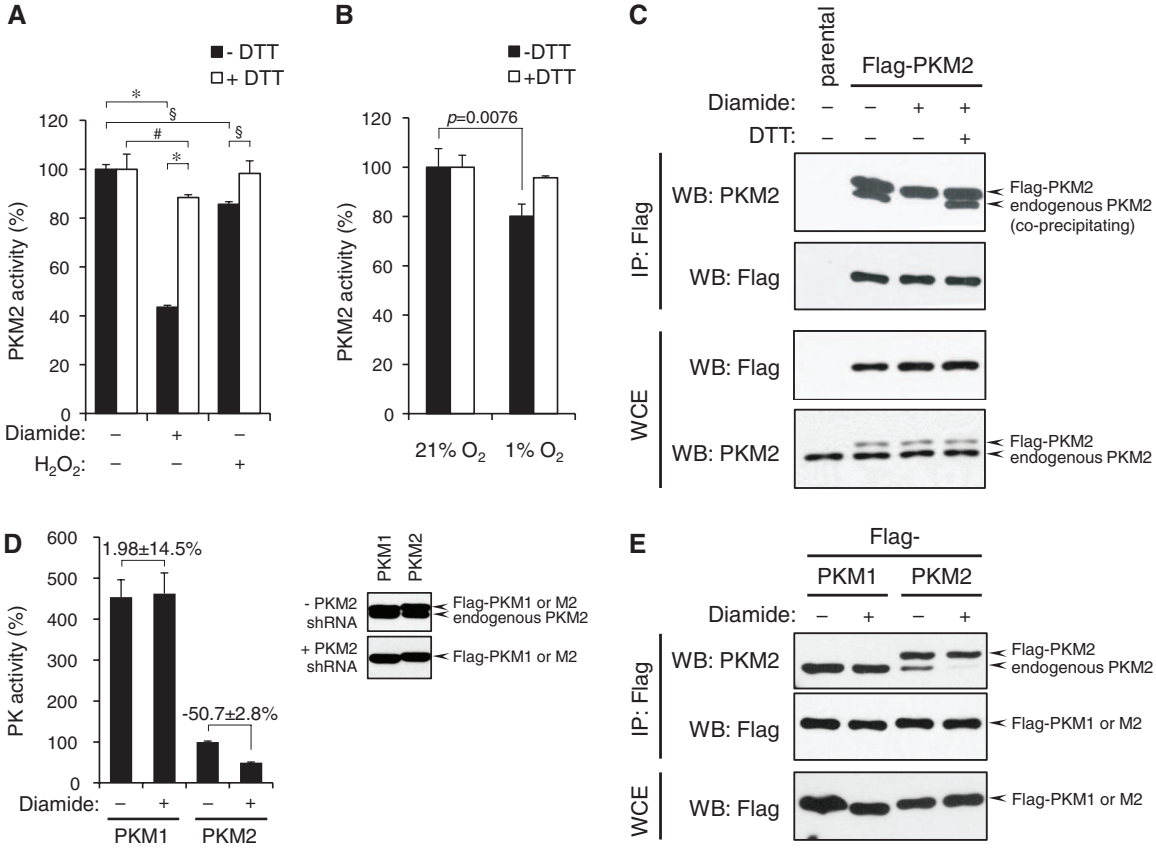

Fig. 1. ROS-promoted dissociation of PKM2 subunits and inhibition of enzymatic activity. (**A**) A549 human lung cancer cells were treated with 250 μM diamide or 1 mM H_2O_2 for 15 min. After cell lysis, pyruvate kinase activity was assayed in the presence or absence of DTT. Percent PKM2 activity (mean ± SD) relative to untreated cells for each condition is shown [*P < 0.001, §P < 0.01, #P < 0.05, two-way analysis of variance (ANOVA) with Bonferroni posttests, n = 3]. (**B**) A549 cells were cultured in a medium containing 5.6 mM glucose for 3 hours under 21% O_2 or 1% O_2. After cell lysis, PKM2 activity was assayed as in (A) (Student's t test, n = 3). (**C**) A549 cells were engineered to express Flag-PKM2 (arrows). Cells were left untreated or were diamide-treated as in (A), and equal portions of lysates prepared under nonreducing conditions were supplemented with or without DTT (1 mM final concentration). Lysates were then subjected to immunoprecipitation with Flag antibody covalently coupled to agarose beads in the presence or absence of DTT, followed by SDS-PAGE and Western blot. (**D**) A549 cells expressing Flag-PKM1 or Flag-PKM2 in the absence of endogenous PKM2 (referred to in the text as Flag-PKM1/kd or Flag-PKM2/kd) were generated as in (*17*). (Right) Expression of Flag-tagged proteins and depletion of endogenous PKM2 were confirmed by Western blot with an antibody recognizing both PKM1 and PKM2. (Left) Lysates of diamide-treated (250 μM, 15 min) cells were prepared and assayed for pyruvate kinase activity as in (A). Percent pyruvate kinase activity (mean ± SD) for each condition relative to untreated Flag-PKM2/kd cells is shown. Numbers denote percent difference in PK activity ± SD between diamide-treated and nontreated Flag-PKM1/kd or Flag-PKM2/kd cells, respectively. (**E**) A549 cells expressing Flag-PKM1 or Flag-PKM2 were treated with diamide (250 μM, 15 min) and, after cell lysis, immunoprecipitation to assess the amount of endogenous PKM2 associated with the tagged PKM isoforms was performed as in (C).

(Fig. 1C). These results indicate either that oxidative stress induces PKM2 subunits to dissociate in vivo or that it makes subunit association less stable during cell lysis and immunoprecipitation. In either event, this change in association of PKM2 subunits after diamide treatment correlated with decreased enzymatic activity.

We examined whether diamide treatment differentially affected PKM2 versus PKM1 activity by assaying pyruvate kinase activity in lysates from cells engineered to express equivalent amounts of either Flag-PKM1 or Flag-PKM2 with concomitant depletion of endogenous PKM2 by short hairpin RNA (henceforth referred to as Flag-PKM1/kd cells or Flag-PKM2/kd cells, respectively; kd for knockdown). Unlike that of PKM2, the activity of PKM1 did not change after diamide treatment (Fig. 1D). Consistent with this observation, formation of complexes between Flag-PKM1 and endogenous PKM2 (using cells still expressing endogenous PKM2) was unaffected by diamide (Fig. 1E). This result suggests that the heteromultimer of PKM1 and PKM2 is protected from oxidation-dependent destabilization.

To assess a possible covalent modification of PKM2, we treated A549 cells with or without diamide and subjected cell lysates to SDS–polyacrylamide gel electrophoresis (SDS-PAGE) under nonreducing conditions. Subsequent protein immunoblot analysis revealed that some PKM2 from diamide-treated cells migrated faster (Fig. 2A, top). This faster-migrating form was not observed when SDS-PAGE was done under reducing conditions (Fig. 2A, bottom). Cysteine residues are particularly prone to oxidation because the sulfhydryl group reacts with various oxygen species, and this reactivity can be influenced by the local protein microenvironment (*26*). Structural analysis of PKM2 revealed three cysteine residues that could affect subunit interaction, enzymatic activity, or both. Cys^{31} and Cys^{424} are located at the subunit interaction interface whereas Cys^{358} is located in a β barrel that includes residues essential for catalytic activity (fig. S2, A and B) (*27*). Replacement of Cys^{358} with Ser^{358} (C358S) abrogated the faster-migrating PKM2 band (Fig. 2B, top), but mutation of Cys^{31} or Cys^{424} did not (fig. S2C).

Lysis of cells under denaturing conditions in the presence of maleimide to block reduced cysteines in proteins, followed by reduction of oxidized cysteines and labeling with biotin-maleimide, allows the detection of oxidized proteins with streptavidin (*24*). Using this method, we detected biotin-labeled Flag-PKM2 in lysates of diamide-treated cells but not in those of control cells (Fig. 2B, bottom). In contrast, we did not detect biotinylated Flag-PKM2(C358S). Furthermore, unlike Flag-PKM2, Flag-PKM2(C358S) still associated with endogenous PKM2 after diamide treatment (Fig. 2C), and the enzymatic activity of the C358S mutant was less sensitive to oxidant-induced inhibition (Fig. 2D). These results indicate that although oxidation of other Cys residues in PKM2 may have minor effects on PKM2 catalytic activity, oxidation of Cys^{358} primarily accounts for ROS-induced inactivation.

Small-molecule activators selectively increase the activity of PKM2 with no effects on PKM1 (*28*). Treatment of purified recombinant PKM2 with the small-molecule PKM2 activator DASA-10 (NCGC00181061, a substituted *N,N′*-diarylsulfonamide) (fig. S3A) prevented inhibition of PKM2 by H_2O_2 (fig. S3B). Incubation of A549 cells with 20 μM DASA-10 caused a 2.8-fold increase in enzyme activity in the absence of diamide and prevented the diamide-induced inhibition of PKM2 activity (fig. S3C and Fig. 2E). Furthermore, DASA-10 preserved the coprecipitation of endogenous PKM2 with Flag-PKM2 after treatment of cells with diamide (Fig. 2F).

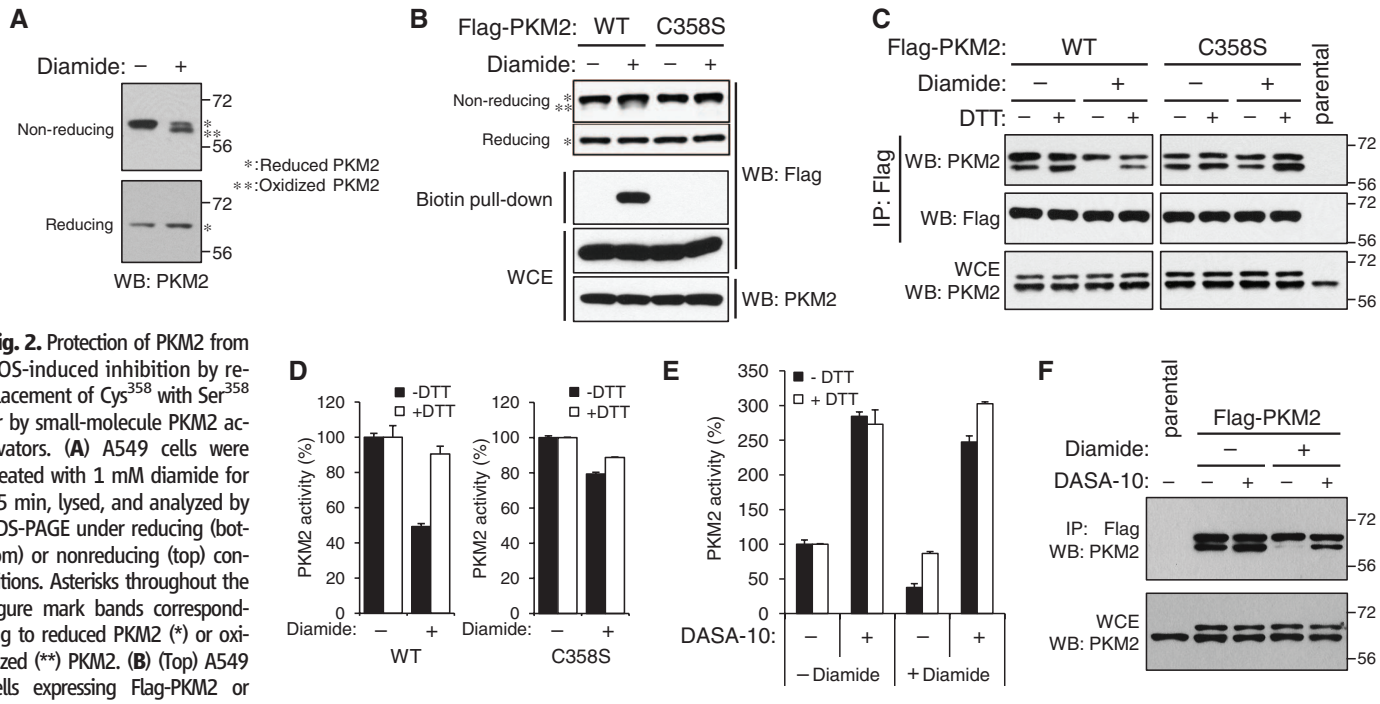

Fig. 2. Protection of PKM2 from ROS-induced inhibition by replacement of Cys^{358} with Ser^{358} or by small-molecule PKM2 activators. (**A**) A549 cells were treated with 1 mM diamide for 15 min, lysed, and analyzed by SDS-PAGE under reducing (bottom) or nonreducing (top) conditions. Asterisks throughout the figure mark bands corresponding to reduced PKM2 (*) or oxidized (**) PKM2. (**B**) (Top) A549 cells expressing Flag-PKM2 or Flag-PKM2(C358S) were treated with 250 μM diamide for 15 min, lysed, and analyzed by SDS-PAGE under reducing or nonreducing conditions. (Bottom) A549 Flag-PKM2/kd or Flag-PKM2(C358S)/kd cells were treated with diamide as above. Oxidized proteins were labeled with biotin-maleimide (*24*), purified with streptavidin-sepharose beads and probed for the presence of Flag-PKM2 or Flag-PKM2(C358S) with Flag antibody. WT, wild type. (**C**) A549 cells expressing Flag-PKM2 or Flag-PKM2(C358S) were treated with 250 μM diamide for 15 min, lysed without DTT, and split into equal portions that were supplemented with or without DTT (1 mM final concentration). After immunoprecipitation with Flag antibody covalently coupled to agarose beads, immunoprecipitates were analyzed by reducing SDS-PAGE and Western blot with the indicated antibodies. (**D**) A549 Flag-PKM2/kd or Flag-PKM2(C358S)/kd cells were treated with diamide as in (C), and pyruvate kinase activity was assayed in cell lysates in the presence or absence of 1 mM DTT. Percent PKM2 activity (mean ± SD) relative to untreated cells for each condition is shown. (**E**) Medium containing 20 μM PKM2 activator DASA-10 (*28*) was added to A549 cells at time $t = -1$ hour; diamide was then added directly to the media at a final concentration of 250 μM at $t = -15$ min. Cells were harvested at $t = 0$, lysed, and pyruvate kinase activity in lysates was assayed in the presence or absence of 1 mM DTT. PKM2 activity is shown as in (D). (**F**) A549 cells expressing Flag-PKM2 were treated with DASA-10 and diamide as in (E) and the respective lysates were subjected to immunoprecipitation with Flag antibody covalently coupled to agarose beads under nonreducing conditions. Immunoprecipitates were analyzed by reducing SDS-PAGE, followed by Western blot with a PKM2 antibody.

Addition of DASA-10 after lysis of diamide-treated cells was less effective in restoring PKM2 activity (fig. S3D). The activator likely maintains PKM2 in an active conformation and thus prevents oxidation of Cys^{358}; however, PKM2 oxidation before addition of activator impairs the ability of the activator to increase the enzymatic activity of PKM2. Likewise, despite the presence of Cys^{358} in PKM1, the failure of this isoform to be inhibited by diamide (Fig. 1D), could be explained by residues in PKM1 that stabilize the active tetramer and thereby block access of ROS to Cys^{358}.

To gain insights into the functional consequences of PKM2 inhibition under oxidative stress, we investigated changes in cellular metabolism after diamide treatment in the presence or absence of DASA-10 (fig. S4). We monitored the flux of glucose into the pentose phosphate pathway (PPP), which produces NADPH for ROS detoxification (*14*, *15*, *29*). Diamide treatment stimulated PPP-dependent $^{14}CO_2$ production from [1-^{14}C]glucose ($P = 0.02$) in A549 cells (Fig. 3A), which indicated that flux into the oxidative branch of the PPP was enhanced in response to oxidative stress (*15*, *29*). In the presence of DASA-10, diamide did not cause a significant increase in PPP-specific $^{14}CO_2$ production (Fig. 3A), which suggested that ROS-dependent inhibition of PKM2 is needed to maintain the availability of glucose-6-phosphate (G-6-P) for flux into the PPP. Consistent with this idea, after 30 min of diamide treatment, the cellular concentration of G-6-P increased 2.3-fold (Fig. 3B). Although this could be a consequence of inhibiting any step in glycolysis or from stimulation of glucose uptake and phosphorylation, the concentration of G-6-P decreased 75.5 ± 17.6% when PKM2 inhibition by diamide was prevented by the presence of DASA-10 (Fig. 3B), which indicated that ROS-induced inhibition of PKM2 may account for the accumulation of G-6-P in response to oxidative stress.

Glucose catabolism via the PPP provides NADPH required for glutathione reductase to generate GSH for ROS detoxification. Cells expressing Flag-PKM2(C358S) in the absence of endogenous PKM2 [henceforth referred to as Flag-PKM2(C358S)/kd cells] had lower amounts of GSH than Flag-PKM2/kd cells (Fig. 3C, left). Similarly, treatment of parental cells with either DASA-10 (Fig. 3C, right) or another structurally related PKM2 activator, DASA-58 (NCGC00185916, ML203) (figs. S3A and S5A) resulted in lower amounts of GSH. This decrease in GSH concentration was not observed in Flag-PKM1/kd cells even after longer periods of activator treatment (fig. S5B). Because PKM1 activity is unaffected by DASA-10 or DASA-58 (*28*), these results indicate that the effects of these compounds on GSH concentration are a consequence of PKM2 activation, rather than off-target effects.

To test whether decreased abundance of GSH induced by the PKM2 activators impaired cellular capacity for ROS detoxification, we measured intracellular ROS concentrations after treatment of cells with H_2O_2. H_2O_2 elicited greater accumulation of ROS in PKM2 activator–treated cells than in dimethyl sulfoxide (DMSO)–treated cells, and this difference was more pronounced with increased amounts of H_2O_2 (Fig. 3D and fig. S5C). Genetic replacement of PKM2 with PKM1 in mouse embryo fibroblasts (MEFs) (fig. S6, A and B) resulted in increased accumulation of ROS in H_2O_2-treated cells compared with that in MEFs with intact PKM2 (fig. S6C). Thus, PKM2 inhibition due to oxidative stress contributes to a metabolic response that can deplete ROS.

To test whether this mechanism is relevant for cell survival under oxidative stress, we examined the effects of DASA-10 on diamide- or H_2O_2-induced cell death. In response to treatment with either H_2O_2 or diamide, cell death was increased in PKM2 activator–treated cells compared with DMSO-treated cells (Fig. 4A and fig. S7). Also, Flag-PKM2(C358S)/kd cells were more sensitive to diamide than Flag-PKM2/kd cells (Fig. 4B).

We monitored cell mass accumulation of Flag-PKM2/kd or Flag-PKM2(C358S)/kd cells over several days in an atmosphere of 21% or 1% oxygen to determine whether PKM2 inhibition under conditions of increased endogenous ROS levels induced by hypoxia (fig. S1) was functionally relevant. With standard tissue culture concentrations of glucose (25 mM), the proliferation of the two cell lines was indistinguishable at either 21% oxygen (fig. S8, A and B) or 1% oxygen (fig. S8C). In contrast, when the glucose concentration in the media was reduced to a physiological level of 5.6 mM, Flag-PKM2(C358S)/kd cells showed a modest but reproducible ($P = 0.0041$) decrease in cell mass accumulation (fig. S8D). This was more evident when cells were grown in 1% oxygen (Fig. 4C). Under the same culture conditions, we could detect oxidation of endogenous PKM2 which was diminished when cells were treated with the antioxidant *N*-acetylcysteine (NAC) (fig. S9A). In contrast, we detected neither biotin-maleimide labeling (fig. S9B), nor a significant change in the enzymatic activity of Flag-PKM2(C358S) under hypoxia (fig. S9C). These

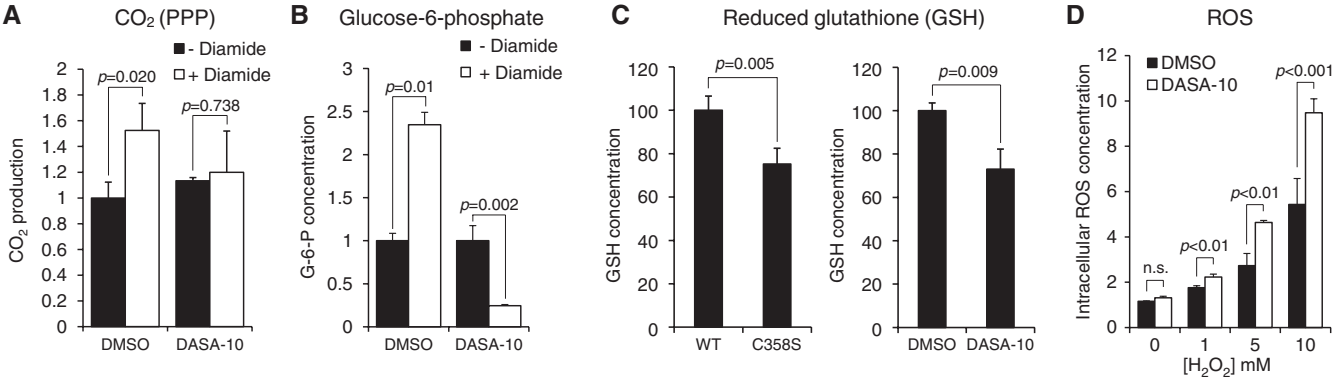

Fig. 3. Changes in glucose metabolism required for cellular antioxidant responses are supported by ROS-induced inhibition of PKM2. (**A**) PPP-dependent glucose oxidation to CO_2. A549 cells were seeded, and after 24 hours, media were supplemented with [1-^{14}C]glucose or [6-^{14}C]glucose plus 10 μM DASA-10 and 100 μM diamide where indicated. Released $^{14}CO_2$ was measured after a 3-hour incubation of cells with labeled glucose. The rate of $^{14}CO_2$ production from glucose via the PPP was calculated as described (*24*). Mean PPP-dependent $^{14}CO_2$ release rates relative to (DMSO, –Diamide) ± SD are shown (Student's *t* test, $n = 3$). (**B**) A549 cells were treated with 10 μM PKM2 activator DASA-10 or DMSO for 1 hour before addition of 250 μM diamide directly into the medium. Cellular metabolites were harvested at $t = 30$ min and analyzed by liquid chromatography coupled to triple quadrupole tandem mass spectrometry (*24*). Bars represent mean concentrations of G-6-P at $t = 30$ min relative to $t = 0$ min ± SD ($n = 3$). Statistical analysis details are described in (*24*). (**C**) Intracellular GSH concentrations of A549 Flag-PKM2/kd and Flag-PKM2(C358S)/kd cells (left panel) or A549 cells treated either with PKM2 activator DASA-10 (10 μM) or DMSO for 1 hour (right panel) were assessed using ThiolTracker violet. Mean GSH concentrations relative to WT or DMSO-treated cells, respectively, are shown (Student's *t* test, $n = 3$). (**D**) After treatment with DMSO or 10 μM PKM2 activator DASA-10 for 1 hour, A549 cells were incubated with the ROS-sensitive fluorescent dye chloromethyl-2′,7′-dichlorofluorescein diacetate (CM-H_2DCFDA), and H_2O_2 was added at the indicated concentrations. Cells were then collected after 15 min, and ROS-dependent fluorescence was measured by flow cytometry. Mean fluorescence intensities ± SD are shown, and *P* values were calculated by two-way ANOVA with Bonferroni posttests ($n = 3$).

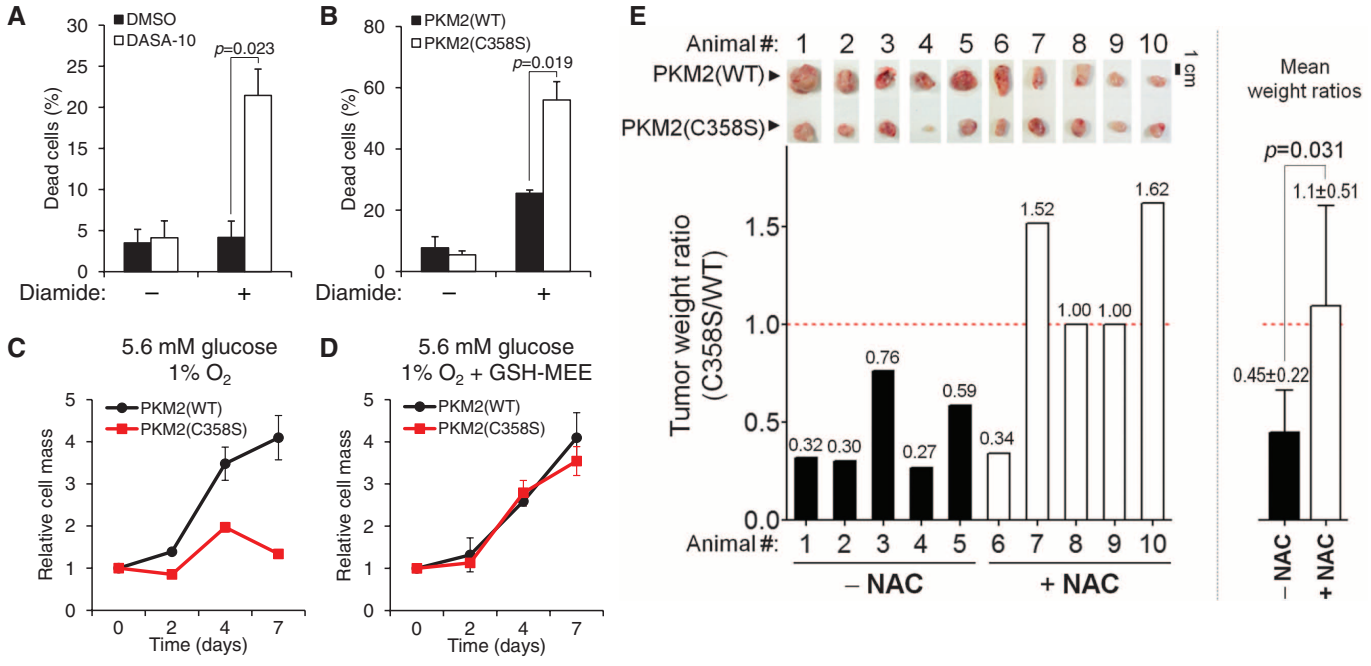

Fig. 4. Promotion of cancer cell survival and tumor growth under oxidative stress by PKM2 inhibition. (**A**) DASA-10 (10 μM) or DMSO was added to H1299 human lung cancer cells at $t = -1$ hour. At $t = 0$, 150 μM diamide was added directly into the medium. At $t = +3$ hours, cells were collected by trypsinization and stained with propidium iodide (PI). Dead (PI-stained) cells were scored by flow cytometry (Student's t test, $n = 3$). (**B**) H1299 Flag-PKM2/kd or H1299 Flag-PKM2(C358S)/kd cells were treated with 150 μM diamide for 3 hours, at which point dead cells were detected as in (A) (Student's t test, $n = 3$). (**C** and **D**) H1299 Flag-PKM2/kd or H1299 Flag-PKM2(C358S)/kd cells were seeded in medium containing 5.6 mM glucose and cultured in 1% O_2 in the absence (C) or presence (D) of 4 mM GSH-MEE. Cells were fixed at the indicated time points, and cell mass was quantified by crystal violet staining (C: $P < 0.0001$, two-way ANOVA, $n = 3$) (*24*). (**E**) Equal numbers of H1299 Flag-PKM2/kd or Flag-PKM2(C358)/kd cells were injected into the left and right flanks, respectively, of immunocompromised mice. Half had access to normal water and the other half to water supplemented with 40 mM NAC throughout the experiment. (Top) Photographs of dissected tumors in pairs. The bar graphs represent tumor weight ratios with corresponding value above each bar (left) and mean weight ratios ± SD (right) (P value calculated by Student's t test).

data indicate that the C358S mutant is refractory to hypoxia-induced oxidation. When the cell-permeable GSH analog glutathione-monoethylester (GSH-MEE) was present in the medium for the duration of the experiment, there was no difference in cell mass accumulation between Flag-PKM2(C358S)/kd cells and wild-type Flag-PKM2(WT)/kd cells (Fig. 4D). Furthermore, a phosphotyrosine-containing peptide with amino acid sequence corresponding to the optimal PKM2 binding motif (*18*) inhibited the activities of both Flag-PKM2 and Flag-PKM2(C358S) to a similar degree (fig. S9D), which suggested that the impaired proliferation of Flag-PKM2(C358S)/kd cells is unlikely to be a result of differential sensitivity to growth factor inhibition of the C358S mutant relative to that of PKM2(WT). Therefore, the diminished proliferation of Flag-PKM2(C358S)/kd cells appears to result from impaired antioxidant capacity. Inhibition of PKM2 after oxidative stress contributes to sustaining cell survival when endogenous ROS accumulate.

To determine whether the proposed role for PKM2 in survival under oxidative stress is relevant in vivo, we injected cells into immunocompromised (*nu/nu*) mice and assayed formation of tumors (fig. S10A). Half the mice were given access to standard water and half to water containing NAC throughout the experiment. Tumors derived from Flag-PKM2(C358S)/kd cells were significantly ($P = 0.011$) smaller compared with those expressing wild-type Flag-PKM2 (Fig. 4E and fig. S10). This difference in tumor growth was alleviated in mice treated with NAC. Thus, regulation of PKM2 via oxidation of Cys^{358} is critical under these conditions for optimal tumor growth.

Cancer cells experience a substantial need for providing reducing power in the form of NADPH to fuel biosynthesis of lipids and nucleotides that are in high demand during proliferation (*16*). Consequently, under conditions of oxidative stress, NADPH supply must be appropriately enhanced in order to sustain proliferation while maintaining ROS homeostasis through GSH. Our data indicate that, besides metabolic reprogramming functions associated with promoting anabolic processes, expression of a specific pyruvate kinase isoform, PKM2, confers additional advantages to cancer cells by allowing them to sustain antioxidant responses and thereby support cell survival under acute oxidative stress. As increasing PKM2 activity would compromise both its proanabolic and antioxidant functions, the use of small-molecule PKM2 activators may be an appropriate approach to interfere with cancer cell metabolism for therapeutic purposes.

References and Notes

1. N. K. Tonks, *Cell* **121**, 667 (2005).
2. K. E. Wellen, C. B. Thompson, *Mol. Cell* **40**, 323 (2010).
3. O. Vafa *et al.*, *Mol. Cell* **9**, 1031 (2002).
4. V. Nogueira *et al.*, *Cancer Cell* **14**, 458 (2008).
5. A. A. Sablina *et al.*, *Nat. Med.* **11**, 1306 (2005).
6. K. Bensaad, E. C. Cheung, K. H. Vousden, *EMBO J.* **28**, 3015 (2009).
7. W. Hu *et al.*, *Proc. Natl. Acad. Sci. U.S.A.* **107**, 7455 (2010).
8. S. Reuter, S. C. Gupta, M. M. Chaturvedi, B. B. Aggarwal, *Free Radic. Biol. Med.* **49**, 1603 (2010).
9. B. Halliwell, *Biochem. J.* **401**, 1 (2007).
10. Z. T. Schafer *et al.*, *Nature* **461**, 109 (2009).
11. K. Ishikawa *et al.*, *Science* **320**, 661 (2008).
12. F. Weinberg *et al.*, *Proc. Natl. Acad. Sci. U.S.A.* **107**, 8788 (2010).
13. A. J. Levine, A. M. Puzio-Kuter, *Science* **330**, 1340 (2010).
14. P. P. Pandolfi *et al.*, *EMBO J.* **14**, 5209 (1995).
15. S. Filosa *et al.*, *Biochem. J.* **370**, 935 (2003).
16. M. G. Vander Heiden, L. C. Cantley, C. B. Thompson, *Science* **324**, 1029 (2009).
17. H. R. Christofk *et al.*, *Nature* **452**, 230 (2008).
18. H. R. Christofk, M. G. Vander Heiden, N. Wu, J. M. Asara, L. C. Cantley, *Nature* **452**, 181 (2008).
19. P. Maeba, B. D. Sanwal, *J. Biol. Chem.* **243**, 448 (1968).
20. B. McDonagh, S. Ogueta, G. Lasarte, C. A. Padilla, J. A. Bárcena, *J. Proteomics* **72**, 677 (2009).
21. D. A. Butterfield, R. Sultana, *J. Alzheimers Dis.* **12**, 61 (2007).
22. R. C. Cumming *et al.*, *J. Biol. Chem.* **279**, 21749 (2004).
23. J. K. Brunelle *et al.*, *Cell Metab.* **1**, 409 (2005).
24. Materials and methods are available as supporting material on *Science* Online.
25. E. Eigenbrodt, M. Reinacher, U. Scheefers-Borchel, H. Scheefers, R. Friis, *Crit. Rev. Oncog.* **3**, 91 (1992).
26. Y. M. Janssen-Heininger *et al.*, *Free Radic. Biol. Med.* **45**, 1 (2008).
27. J. D. Dombrauckas, B. D. Santarsiero, A. D. Mesecar, *Biochemistry* **44**, 9417 (2005).

28. M. B. Boxer *et al.*, *J. Med. Chem.* **53**, 1048 (2010).
29. C. Le Goffe *et al.*, *Biochem. J.* **364**, 349 (2002).

Acknowledgments: We thank V. Toxavidis and J. Tigges (Beth Israel Deaconess Medical Center flow cytometry facility) for support with flow cytometry applications; X. Yang and S. Breitkopf for technical assistance with mass spectrometry; Ross Dickins and Scott Lowe (Cold Spring Harbor Laboratory) for the gift of tamoxifen-inducible Cre-expressing retroviral plasmid; and C. Benes, N. Wu, A. Shaywitz, B. Emerling, A. Saci, G. DeNicola, K. Courtney, A. Couvillon, S. Soltoff, A. Carracedo, A. Grassian, J. Brugge, and members of the Cantley lab for helpful discussions. L.C.C. is a cofounder of Agios Pharmaceuticals, a company that seeks to develop novel therapeutics that target cancer metabolism. G.P. is a Pfizer Fellow of the Life Sciences Research Foundation. A.T.S. is a Genentech Fellow and supported by the Japanese Society for the Promotion of Science and the Kanae Foundation for Research Abroad. M.G.V.H. is supported by the NIH (R03MH085679 and 1P30CA147882), the Burroughs Wellcome Fund, the Damon Runyon Cancer Research Foundation, and the Smith family. This work was supported by grants from the NIH (R01-GM056203-13, P01-CA089021, and P01-CA117969-04 to L.C.C), the Starr Cancer Consortium (L.C.C. and M.G.V.H.), the Molecular Libraries Initiative of the National Institutes of Health Roadmap for Medical Research, and the Intramural Research Program of the National Human Genome Research Institute, NIH (M.B.B., J. J., M.S., D.S.A., and C.J.T.). We apologize to colleagues whose work we could not cite because of space limitations.

Supporting Online Material
www.sciencemag.org/cgi/content/full/science.1211485/DC1
Materials and Methods
Figs. S1 to S10
References

20 July 2011; accepted 24 October 2011
Published online 3 November 2011;
10.1126/science.1211485

Hemoglobins S and C Interfere with Actin Remodeling in *Plasmodium falciparum*–Infected Erythrocytes

Marek Cyrklaff,[1]* Cecilia P. Sanchez,[1] Nicole Kilian,[1] Cyrille Bisseye,[2] Jacques Simpore,[2] Friedrich Frischknecht,[1] Michael Lanzer[1]*

The hemoglobins S and C protect carriers from severe *Plasmodium falciparum* malaria. Here, we found that these hemoglobinopathies affected the trafficking system that directs parasite-encoded proteins to the surface of infected erythrocytes. Cryoelectron tomography revealed that the parasite generated a host-derived actin cytoskeleton within the cytoplasm of wild-type red blood cells that connected the Maurer's clefts with the host cell membrane and to which transport vesicles were attached. The actin cytoskeleton and the Maurer's clefts were aberrant in erythrocytes containing hemoglobin S or C. Hemoglobin oxidation products, enriched in hemoglobin S and C erythrocytes, inhibited actin polymerization in vitro and may account for the protective role in malaria.

The malaria parasite *Plasmodium falciparum* has exerted a selective pressure on the human population that has led to the emergence of several polymorphisms within the human genome that protect carriers from severe malaria-related disease and death (*1*). The best-known examples are the structural hemoglobinopathies S (sickle cell trait; HbS) and C (HbC), in which glutamate at the sixth position within the β-globin chain is replaced by valine and lysine, respectively (*2*, *3*). Protection against severe malaria correlates with a distorted display of parasite-encoded adhesins on the surface of infected erythrocytes (*4*, *5*). By reducing the cytoadhesive capacity of parasitized erythrocytes, HbS and HbC seem to mitigate the life-threatening complications resulting from the sequestration of infected erythrocytes in postcapillary microvessels of the brain and other organs. How HbS and HbC bring about this effect is unclear. We tested the hypothesis that HbS and HbC interfere with the machinery that directs parasite-encoded proteins to the erythrocyte surface.

Human erythrocytes lack a secretory system and are rapidly cleared from circulation by the spleen when damaged or infected. To develop within human erythrocytes and to avoid passage through the spleen, *P. falciparum* extensively modifies its host cell (*6*), for example, by placing the disease-mediating immunovariant adhesin PfEMP1 in knob-like protrusions in the erythrocyte plasma membrane (*7*). To direct PfEMP1 and other determinants of virulence and pathology to the erythrocyte's plasma membrane, the parasite establishes a trafficking system within the cytoplasm of its host cell, of which a prominent feature are Maurer's clefts, unilamellar membrane profiles that serve as intermediary compartments for proteins en route to the erythrocyte surface (*8*–*10*). To better define the elements of this machinery and how they are altered when *P. falciparum* develops in HbS and HbC erythrocytes, we applied electron tomography to parasitized erythrocytes preserved by rapid freezing (fig. S1).

We initially investigated *P. falciparum*–infected erythrocytes (at the trophozoite stage, 20 to 26 hours after invasion) containing the wild-type hemoglobin HbA (homozygous). The tomograms revealed the erythrocyte plasma membrane, the knobs, and the Maurer's clefts (Fig. 1A). In addition, we observed an extended network of long, sometimes branched filaments that connected the Maurer's clefts with the knobs. Of the 20 knobs identified in 12 tomograms, all were connected to Maurer's clefts by filaments. The filaments were between 40 and 950 nm long (Fig. 1B) and 6.8 ± 0.5 nm in diameter (Fig. 1C). Some of the filaments branched at main angles of 70° ± 5° and 110° ± 5° (Fig. 1D).

The tomograms further revealed vesicles of various sizes, ranging from 20 nm to more than 200 nm in diameter (fig. S2). About 70% of the observed vesicles (47 out of 68) were attached to filaments (Fig. 1E), independent of their size. The remaining vesicles were associated with Maurer's clefts or appeared free in the erythrocyte cytosol. Some vesicles carried PfEMP1 (Fig. 1F) (*9*, *11*).

Tomograms taken in areas more than 5 μm distant from Maurer's clefts also revealed vesicles and a filamentous network (Fig. 2A). However, these filaments were shorter than those observed in the vicinity of Maurer's clefts (Fig. 1B). Moreover, the two main branching angles of the filaments were equally distributed, whereas close to Maurer's clefts the filaments preferentially branched at an angle of 70° ± 5° in the direction of the Maurer's clefts (Fig. 1D).

The filaments had features reminiscent of actin filaments, including diameter and branching pattern (Fig. 1, C and D) (*12*). Indeed, treating *P. falciparum*–infected erythrocytes (trophozoites) for 10 min with the actin depolymerizing agent cytochalasin D (1 μM) destroyed the filaments and altered the morphology of the Maurer's clefts (Fig. 2B). Vesicles were also not observed under these conditions. Immunolabeling of high-pressure frozen electron microscopy (EM) sections, using a gold-coupled monoclonal antibody specific for β-actin (*13*), provided further evidence that the long filaments contained actin (Fig. 2C and fig. S3). We noted a higher density of actin labeling in the area between the Maurer's clefts and the erythrocyte plasma membrane compared with areas elsewhere in the erythrocyte cytoplasm (fig. S3), supporting the conclusion that actin filaments connect the Maurer's clefts with the erythrocyte plasma membrane (*13*). Ankyrin may anchor the actin filaments to the Maurer's clefts (*14*).

The erythrocyte owes its shape and physical properties to a membrane skeleton that is primarily composed of spectrin tetramers joined by a junctional complex that is mainly composed of actin protofilaments (*15*). The length of the actin protofilaments is tightly regulated and is restricted to 14 to 16 monomers (*15*). Tomograms

[1]Department of Infectious Diseases, Parasitology, Heidelberg University, Im Neuenheimer Feld 324, 69120 Heidelberg, Germany. [2]Biomolecular Research Center Pietro Annigoni, 01 BP 364 Ouagadougou, Burkina Faso.

*To whom correspondence should be addressed. E-mail: michael_lanzer@med.uni-heidelberg.de (M.L.); marek.cyrklaff@med.uni-heidelberg.de (M.C.)